Volume 25
Number 2
14 January 2023
Pages 175–338

CrystEngComm

rsc.li/crystengcomm

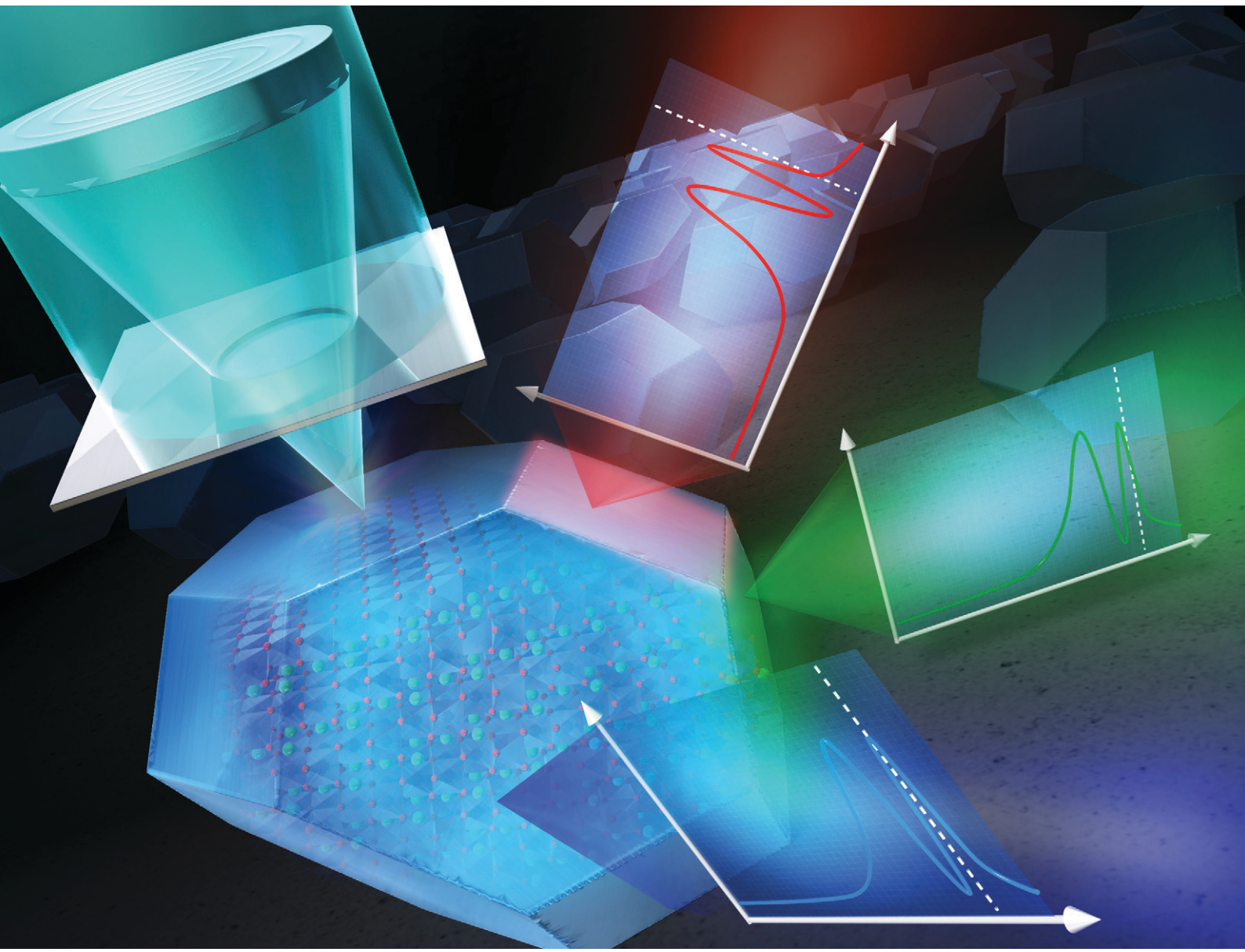

ISSN 1466-8033

ROYAL SOCIETY OF CHEMISTRY

PAPER

Eiji Hosono, Yoshihisa Harada *et al.*

Facet-dependent electrochemical performance and electronic structure of $LiCoO_2$ polyhedral particles revealed by microscopic resonant X-ray photoelectron spectroscopy

CrystEngComm

PAPER

View Article Online
View Journal | View Issue

Cite this: *CrystEngComm*, 2023, **25**, 183

Facet-dependent electrochemical performance and electronic structure of $LiCoO_2$ polyhedral particles revealed by microscopic resonant X-ray photoelectron spectroscopy†

Wenxiong Zhang, [a] Eiji Hosono, *[bcd] Daisuke Asakura, [bcd] Shingo Tanaka, [be] Masaki Kobayashi, [fg] Naoka Nagamura, [hkl] Masaharu Oshima, [i] Jun Miyawaki, [aij] Hisao Kiuchi [ai] and Yoshihisa Harada *[adi]

The morphology of active material particles has a significant impact on the charge–discharge cycle performances of lithium-ion batteries because each crystal surface constructed by different elemental arrangements indicates various surface energies. The surface properties of each facet affect the stability of the interface between the facets of particles and electrolytes. In this study, we applied microscopic resonant photoelectron spectroscopy with a spatial resolution of 100 nm (3DnanoESCA system) to reveal the electronic structure of each facet of prototypical layered $LiCoO_2$ cathode particles, where the characteristic facets are (001), (104), and (012). We detected the difference in an electronic structure near the valence-band maximum (around 1–3 eV) on different $LiCoO_2$ facets, where the dominant Co 3d bands at the valence band of the (001), (104) and (012) facets showed binding energies of 2.48, 2.25 and 2.02 eV, respectively. The closer Co 3d band of the (012) facet to the Fermi level makes it easier to lose electrons than the other facets, suggesting its more reactive property than the other facets. This technique, which provides the electronic structure of each crystal facet, is useful for designing active materials with excellent charge–discharge cycle performances.

Received 29th August 2022,
Accepted 15th October 2022

DOI: 10.1039/d2ce01185a

rsc.li/crystengcomm

[a] *Institute for Solid State Physics (ISSP), The University of Tokyo, 5-1-5 Kashiwanoha, Kashiwa, Chiba 277-8581, Japan. E-mail: harada@issp.u-tokyo.ac.jp*
[b] *Global Zero Emission Research Center, National Institute of Advanced Industrial Science and Technology (AIST), 16-1 Onogawa, Tsukuba, Ibaraki 305-8569, Japan. E-mail: e-hosono@aist.go.jp*
[c] *Research Institute for Energy Conservation, National Institute of Advanced Industrial Science and Technology (AIST), 1-1-1 Higashi, Tsukuba, Ibaraki 305-8565, Japan*
[d] *AIST-UTokyo Advanced Operando-Measurement Technology Open Innovation Laboratory, 5-1-5 Kashiwanoha, Kashiwa, Chiba 277-8565, Japan*
[e] *Research Institute of Electrochemical Energy, National Institute of Advanced Industrial Science and Technology (AIST), 1-8-31, Midorigaoka, Ikeda, Osaka 563-8577, Japan*
[f] *Department of Electrical Engineering and Information Systems, The University of Tokyo, 7-3-1 Hongo, Bunkyo-ku, Tokyo 113-8656, Japan*
[g] *Center for Spintronic Research Network, The University of Tokyo, 7-3-1 Hongo, Bunkyo-ku, Tokyo, Japan*
[h] *Research Center for Advanced Measurement and Characterization, National Institute for Materials Science (NIMS), 1-2-1 Sengen, Tsukuba, Ibaraki 305-0047, Japan*
[i] *Synchrotron Radiation Research Organization, The University of Tokyo, 7-3-1 Hongo, Bunkyo-ku, Tokyo, 113-8656, Japan*
[j] *Institute for Advanced Synchrotron Light Source, National Institutes for Quantum Science and Technology, 6-6-11, Aoba, Sendai, Miyagi, 980-8579, Japan*
[k] *Department of Materials Science, Tokyo University of Science, 6-3-1, Niijuku, Katsushika, Tokyo 125-8585, Japan*
[l] *PRESTO, Japan Science and Technology Agency, 4-1-8, Honcho, Kawaguchi, Saitama 332-0012, Japan*

† Electronic supplementary information (ESI) available. See DOI: https://doi.org/10.1039/d2ce01185a

Introduction

Lithium-ion batteries (LIBs) are expected to be energy storage devices for portable electronic, electrical vehicles/hybrid electric vehicles and smart grid systems. Layered transition metal oxide materials are the most widely commercially used cathode materials for LIBs with high energy density and long cycle life.[1–3] Tremendous efforts have been devoted to achieving a longer cycle life of the layered material.[4–8]

Physical characteristics of primary particles, such as composition, size, and morphology, are anticipated to be important in the cycling life of LIBs.[9–11] The relationship between the surface energy of the primary particle on the cathode and the electrochemical stability has been demonstrated by applying density functional theory (DFT) calculations.[12–15] Elucidating the electronic structure on each facet of the prototypical layered $LiCoO_2$ cathode particle and its correlation with the electrochemical performance are important to fundamentally understand the performance of layered cathode materials of LIBs.

To obtain the element-selective electronic structure of cathode materials, X-ray photoelectron spectroscopy (XPS) has been extensively applied.[16–18] For example, elucidating

the electronic structure changes of the delithiated $LiCoO_2$ cathode material has been widely reported by applying the XPS technique.[18–21] Furthermore, resonant X-ray photoelectron spectroscopy (RXPS) with the synchrotron radiation light source enables us to observe the resonantly enhanced 3d partial density of states (DOS) of transition metal elements.[22,23]

Herein, we report an experimental study to address the electronic structure of the characteristic facets of $LiCoO_2$ polyhedral particles using a microscopic RXPS technique. There are two candidates for $LiCoO_2$ materials with controlled crystal surfaces: epitaxial thin film and powder composed of facets. While the thin film material undergoes strain during lattice matching with the single-crystal substrate, the powder material is preferable for precise electronic structure analysis. However, the particle size of the powder material for practical use is about a micrometer scale. An experimental technique with a spatial resolution as high as ~1 μm is indispensable for the analysis of each facet constituting each particle. Therefore, microscopic photoelectron spectroscopy is considered a powerful experimental approach to elucidate the facet-dependent electronic structure of micron-sized $LiCoO_2$ particles.[20,24] In this study, photoelectron spectral mapping images of the $LiCoO_2$ polyhedral-shaped single crystal have demonstrated that the valence band spectra of $LiCoO_2$ particles change with the facet. The nearer Co 3d valence band of the (012) facet to the Fermi level compared to those of (001) and (104) makes it the most reactive facet of $LiCoO_2$ particles, which could result in the poor cycling performance of LIBs. The surface stability of each facet of a particle was successfully measured using microscopic resonant photoelectron spectroscopy, which can selectively extract the Co 3d electronic structure in the valence band.

Experimental section

A $LiCoO_2$ powder sample was synthesized by applying the molten salt method. NaCl, $LiOH{\cdot}H_2O$ and $Co(NO_3)_2{\cdot}6H_2O$ were mixed and heated at 1000 °C for 5 h in air. Finally, the samples were washed with distilled water and dried under vacuum conditions.

The structure of the powder sample was investigated using powder X-ray diffractometer (XRD) radiation (Bruker, D2 PHASER). The particle size and morphology of the samples were observed using a scanning electron microscope (SEM) (JEOL, JCM-6000Plus).

The facets of the $LiCoO_2$ particles were indicated by SHAPE simulation. SHAPE is a program for drawing the external morphology (facets) of crystals and quasi-crystals.[25] Crystal systems, lattice constants, symmetries, and *d*-spacings for each facet of the $LiCoO_2$ particle are required for the simulation.

The RXPS spectra were measured using a 3DnanoESCA station at BL07LSU in SPring-8. To determine the incident photon energy for the RXPS measurement by utilizing 3DnanoESCA, a Co L-edge X-ray absorption spectroscopy (XAS) spectrum for the $LiCoO_2$ powder sample was measured at the HORNET station at the same beamline. The spot size of the XAS was 5 μm × 30 μm. For the XAS measurement, the total electron yield mode was used, where the probing depth is less than 10 nm. 3DnanoESCA is a microscopic photoelectron spectroscopy technique with spatial resolution better than 100 nm for the element selective chemical analysis. The energy resolution for both the XAS and XPS measurements was about 100 meV. To analyze the Co L-edge XAS spectrum, a charge-transfer multiplet (CTM) calculation was applied.[26]

For sample preparation before RXPS, the $LiCoO_2$ powder sample was pressed into an indium sheet. Then, the indium sheet was mounted on the sample holder using copper conductive tape (Fig. 1a). Finally, the holder was transferred to the main chamber of the 3DnanoESCA. For RXPS on the 3DnanoESCA station,[27] synchrotron radiation (SR) soft X-ray was focused on by employing a Fresnel zone plate (FZP) and an order-sorting pinhole aperture (OSA) of 80 μm, as shown in Fig. 1a. Photoelectrons were detected using a modified angle-resolved photoelectron spectrometer (VG Scienta

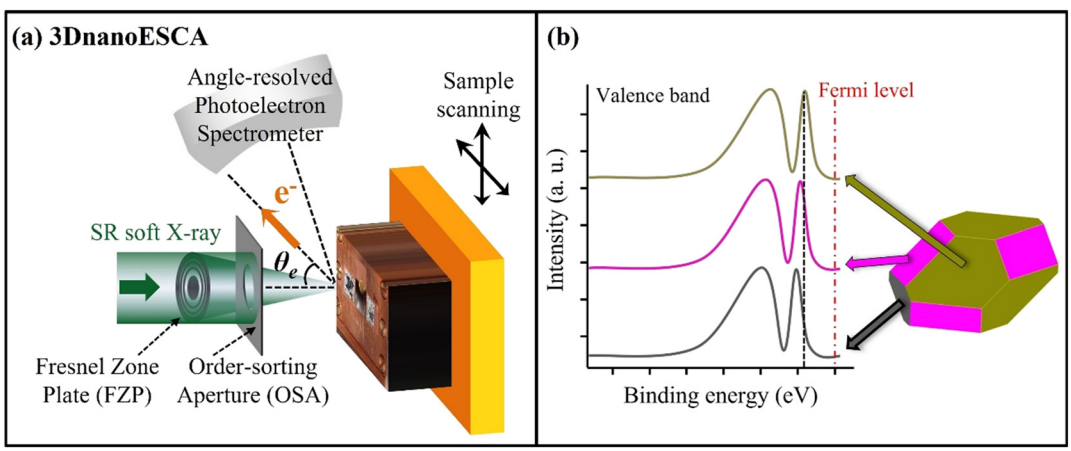

Fig. 1 Schematic images for (a) 3DnanoESCA system and (b) facet-dependent valence band analysis of particle by microscopic XPS using 3DnanoESCA.

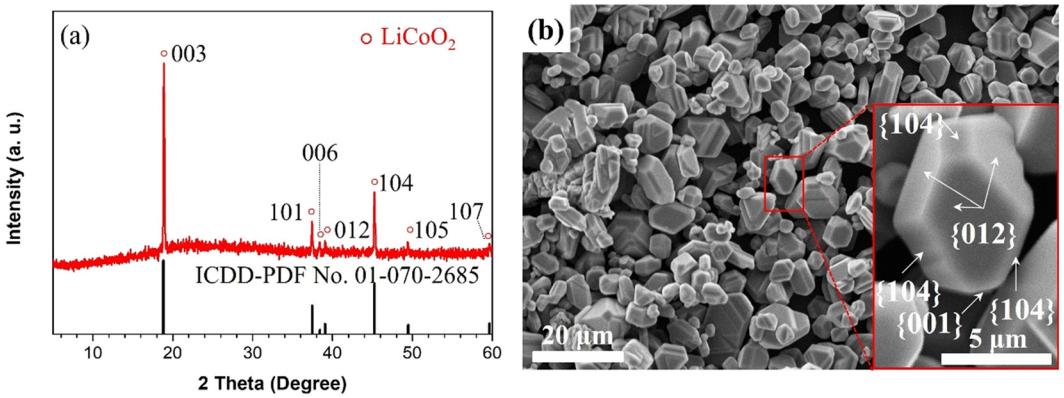

Fig. 2 (a) XRD pattern and (b) SEM images of $LiCoO_2$ particles obtained by employing the molten salt method. The inset shows an enlarged picture of a particle comprising {001}, {104}, and {012} facets.

R3000-EWAL) with a pass energy of 200 eV (Fig. 1a). It can achieve 3D spectral imaging with an in-plane spatial resolution of better than 100 nm.[27] Then, the pinpoint XPS can be conducted at the selected facet of the individual particle (Fig. 1b). A surface clean Au (4f) sample was used for the energy calibration. The background under the XPS spectra was subtracted using a Shirley-type function.

Results and discussion

Fig. 2a shows the XRD pattern and SEM image of the $LiCoO_2$ sample. The XRD pattern indicates the formation of a pure $LiCoO_2$ phase belonging to the rhombohedral space group ($R\bar{3}m$), which agrees well with the international center for the diffraction data (ICDD) pattern. The obtained lattice constants along the (100) and (001) directions are a = 2.816 Å and c = 14.053 Å, respectively, which are consistent with those of a = 2.816 Å and c = 14.054 Å in the ICDD-Pair Distribution Function (PDF) data, respectively.[28] Fig. 2b shows the SEM image of the single crystalline $LiCoO_2$ particles. The $LiCoO_2$ particles clearly have facets, and the particle sizes range from 5 to 10 μm. Given that the spatial resolution of the 3DnanoESCA is more than 100 nm, particles with surface areas over μm^2 on each facet of $LiCoO_2$ can be well distinguishable after mapping, where the pinpoint RXPS can be conducted on each characterized facet.

To determine the resonant energy of Co for RXPS, the Co L-edge XAS spectrum was measured, as shown in Fig. 3a. The spectrum indicates the average information of the Co L-edge XAS for the $LiCoO_2$ powder sample. There are two main peaks of L_3 and L_2 edges that are due to the electronic transitions from the Co $2p_{3/2}$ and $2p_{1/2}$ core levels (split by the spin–orbit interaction) to unoccupied 3d orbitals hybridized with O 2p orbitals, respectively.[15] It is well known that the absorption peaks are relatively intense owing to the electronic dipole allowing 2p to 3d transitions and are

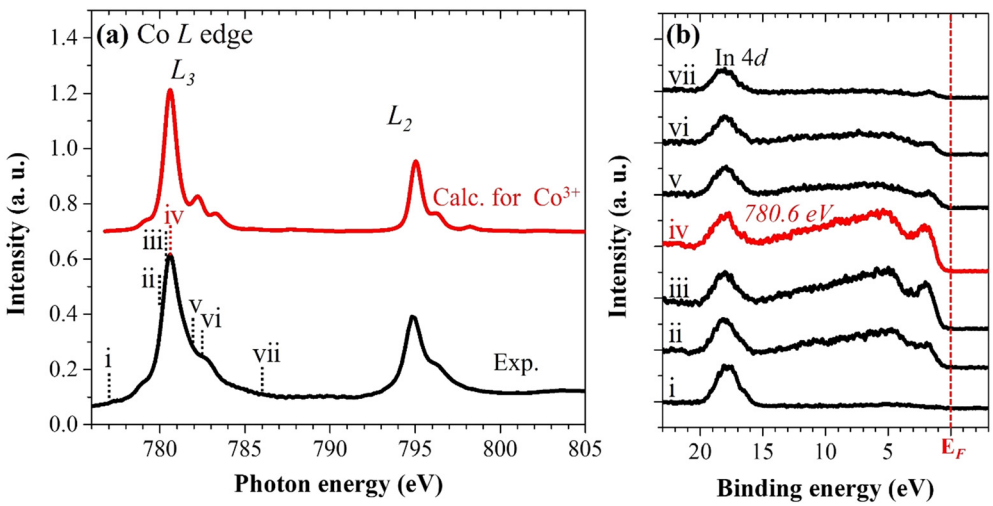

Fig. 3 (a) Co L-edge XAS spectrum for the $LiCoO_2$ powder sample and calculated spectrum for Co^{3+} state. In the CTM calculation, the CoO_6 octahedron with the O_h symmetry is considered. Some of the electronic structure parameters are determined as follows: crystal-field splitting 10Dq = 1.4 eV, charge-transfer energy from the O 2p to Co 3d orbitals Δ = 0.6 eV, coulomb repulsion of d-electrons U_{dd} = 6.5 eV, core-hole potential U_{pd} = 7.5 eV, hopping parameter values $T(e_g)$ = 2.0 eV and $T(t_{2g})$ = 1.0 eV. (b) RXPS spectra were measured with varying photon energies indicated by i to vii, as shown in (a), by direct beams on particles without an X-ray condenser.

sensitive to the oxidation state, spin state, and bond covalency. According to the CTM calculation in Fig. 3(a) and previous XAS reports,[29,30] the Co L-edge XAS spectrum is attributed to Co^{3+} low-spin state.

With the selected photon energies from the XAS spectrum, the RXPS measurement was conducted with 3DnanoESCA using the beam without focusing on the FZP and OSA. The average XPS spectrum included signals from the indium sheet, in addition to those from the $LiCoO_2$ particles. Fig. 3b shows the valence band XPS spectra obtained with several incident energies. It is noteworthy to mention that the prominent enhancement of the X-ray photoelectron spectra was obtained with a photon energy of 780.60 eV, corresponding to the Co L_3-edge main peak in the XAS spectrum. In the RXPS spectra, the peaks around 18.2 eV in the binding energy scale were attributed to the In 4d orbital originating from the indium sheet used to hold the $LiCoO_2$ particles.

Fig. 4b shows the O 1s photoelectron intensity mapping image of the particle, which was selected based on the observation (Fig. 4a) by an optical microscope. The photoelectron intensity mapping image of the O 1s (around 450–470 eV (kinetic energy)) of the $LiCoO_2$ particle is obtained by applying 3DnanoESCA with a photon energy of 1000 eV. The spatial resolution of the mapping is comparable with the SEM image (Fig. 4c), which was observed after the 3DnanoESCA analysis. The polyhedron-like particle with clear facets can be observed, and the corresponding facets are indicated to be {001}, {104}, and {012} by the SHAPE simulation,[25] as shown in Fig. 4d. The intensity of the left side of the image was brighter than that of the right side. This is due to the influence of geometrical relationships between the photoelectron analyzer and the incident beam spot on the sample (Fig. 1a).[20,24]

Subsequently, the pinpoint RXPS spectra were measured at the marked points of each facet, as shown in Fig. 4b, with a photon energy of 780.60 eV. Fig. 4e shows the pinpoint RXPS spectra corresponding to points 1–3. Near the valence-band maximum (around 1–3 eV), prominent peaks in the Co 3d RXPS spectra are observed, whereas in the region between 3 and 10 eV, the direct O 2p and O 2p/Co 3d-like contributions are dominant.[17] Schmeißer *et al.* demonstrated similar valence band spectra of $LiCoO_2$ thin film using RXPS.[31] It has been reported that the Co 3d and O 2p states contribute to DOS in the valence band, whereas the contributions of the Li 2s/2p states are negligible.[17] As shown in Fig. 4e, the binding energy of the Co 3d peak from point 1 indicated by the (001) facet (2.48 eV) is higher than that from point 2 indicated by the (104) facet (2.25 eV). Interestingly, the Co 3d state from point 3 indicated by the (012) facet shows the lowest binding energy of 2.02 eV, which is nearest to the Fermi level. Similarly, the trend of Co 3d binding energies corresponding to each facet agrees with the different particles, as shown in Fig. S1.† In addition, in Fig. S1,† it is noted that the In 4d peaks (around 18.2 eV) from each facet showed no shift. Thus, there is no charge up during the RXPS measurement. The results demonstrate the facet-dependent valence band of $LiCoO_2$. It is noteworthy to mention that the facet-dependent electronic structure of $LiCoO_2$ particles was experimentally presented for the first time herein owing to the high spatial resolution of the 3DnanoESCA system.

It has been reported that $LiNi_xCo_yMn_{1-x-y}O_2$ particles,[11] which have a similar crystal structure to the $R\bar{3}m$ space group, with the (012)-dominated facet showed low cycle performance compared to the (001) or (104) facet-dominated particles, which can also be explained by our results. The highly reactive (012) facet-dominated particle can easily react with the electrolyte during cycling, thereby causing the degradation of the cycling performance of LIBs.[11] In general, the nucleophilicity of oxygen on the metal oxide surface is higher owing to the increase in electronegativity and covalency of the M–O bond. It has been reported that for late transition metal oxides, the smaller gap between the Fermi level and the O 2p band, which is hybridized with the Co 3d orbital, could increase the nucleophilicity of oxygen on the electrode surface.[32] It is considered that the unstable energy

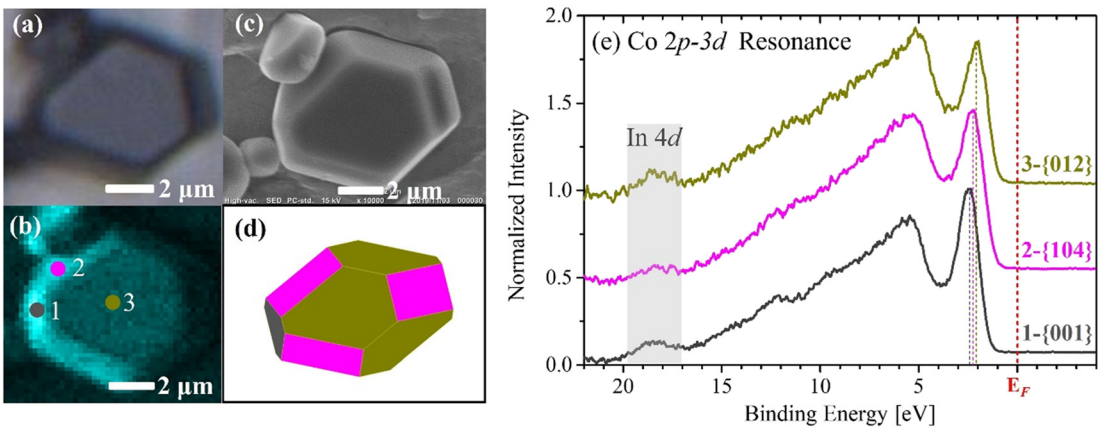

Fig. 4 (a) 2D optical microscope image, (b) O 1s photoelectron intensity mapping image, and (c) SEM image of a $LiCoO_2$ particle. (d) SHAPE simulation of the $LiCoO_2$ particle with indicative facets. (e) Facet-dependent RXPS of the $LiCoO_2$ particle with a photon energy of 780.60 eV.

level of oxygen in the covalent bonding of the M–O bond causes the low cycling performance of the LIBs.

However, according to the calculation by Hong *et al.*,[15] the surface energy of the (001), (104), and (012) facets of the $LiCoO_2$ particle were calculated to be 1.040, 0.791 and 1.652 J m^{-2}, respectively. Among these, the surface energies of (012) and (104) are the highest and lowest, respectively, suggesting that they are the least and most thermodynamically favorable surfaces. The (001) and (104) facets are more stable than the (012) facet. The surface atomic arrangements for each facet are shown in Fig. S2.† In the abovementioned case of the $LiNi_xCo_yMn_{1-x-y}O_2$ cathode, the higher reactivity of the (012) facet showing the least stability during electrochemical cycling than that of (001) and (104) facets could be attributed to the higher surface energy.[11] In our study, the lowest binding energy of Co 3d of the (012) facet compared to that of the (001) and (104) facets was clarified. A possible correlation between the surface energy and the valence band structure of $LiCoO_2$ is addressed in this study. The higher surface energy corresponds to a lower binding energy of the Co 3d level, suggesting higher reactivity during electrochemical cycling. These reports are consistent with our discussion that the Co 3d band closer to the Fermi level, such as the (012) facet, is an unstable facet. In developing materials with high properties for LIBs, it is very important to obtain experimental support using microspectroscopy.

Conclusions

We studied the electronic structure on the equilibrium (001), (104), and (012) facets of $LiCoO_2$ particles by RXPS using the 3DnanoESCA system with 100 nm spatial resolution. For the first time, the facet-dependent electronic structure in the valence band of the $LiCoO_2$ particle was experimentally obtained. A dominated Co 3d band at the valence band from the (001), (104), and (012) facets of $LiCoO_2$ show the binding energies of 2.48 eV, 2.25 eV, and 2.02 eV, respectively. The lowest binding energy of the (012) facet toward the Fermi level makes it easier to lose electrons. The results shown in this study provide solid evidence to explain the instability of the charge–discharge cycle of LIB using (012) facet-dominated layered transition metal oxide materials. For the strategy of morphology control to improve the electrochemical performance of active materials for LIBs, microspectroscopy using synchrotron soft X-ray is an important technique.

Author contributions

E. H. and Y. H. conceived, designed, and coordinated the study. E. H. prepared the concerning materials. W. Z. and N. N. conducted the 3DnanoESCA measurement. W. Z., E. H., D. A., S. T., N. N., M. K., M. O., and Y. H. analyzed the data from the 3DnanoESCA measurement. All authors discussed the results and wrote the manuscript.

Conflicts of interest

We declare no conflict of interest.

Acknowledgements

This work was carried out by joint research by the Synchrotron Radiation Research Organization and the Institute for Solid State Physics, The University of Tokyo (Proposal Numbers 2017B7541, 2019A7594, 2019B7470, 2019B7642 and 2020A7471). This work was partially supported by the Spintronics Research Network of Japan (Spin-RNJ).

References

1 J. Qian, L. Liu, J. Yang, S. Li, X. Wang, H. L. Zhuang and Y. Lu, *Nat. Commun.*, 2018, **9**, 1–11.
2 K. Mizushima, P. C. Jones, P. J. Wiseman and J. B. Goodenough, *Mater. Res. Bull.*, 1980, **15**, 783–789.
3 L. Wang, J. Li, X. He, W. Pu, C. Wan and C. Jiang, *J. Solid State Electrochem.*, 2009, **13**, 1157–1164.
4 Y. Lyu, X. Wu, K. Wang, Z. Feng, T. Cheng, Y. Liu, M. Wang, R. Chen, L. Xu and J. Zhou, *Adv. Energy Mater.*, 2020, 2000982.
5 U. Nisar, N. Muralidharan, R. Essehli, R. Amin and I. Belharouak, *Energy Storage Mater.*, 2021, **38**, 309–328.
6 S. Chen, X. Zhang, M. Xia, K. Wei, L. Zhang, X. Zhang, Y. Cui and J. Shu, *J. Electroanal. Chem.*, 2021, **895**, 115412.
7 C. Zhang, W. Jiang, W. He and W. Wei, *Energy Storage Mater.*, 2021, **37**, 161–189.
8 C. Julien, A. Mauger, K. Zaghib and H. Groult, *Materials*, 2016, **9**, 595.
9 J.-N. Zhang, Q. Li, C. Ouyang, X. Yu, M. Ge, X. Huang, E. Hu, C. Ma, S. Li, R. Xiao, W. Yang, Y. Chu, Y. Liu, H. Yu, X.-Q. Yang, X. Huang, L. Chen and H. Li, *Nat. Energy*, 2019, **4**, 594–603.
10 S. Liu, L. Xiong and C. He, *J. Power Sources*, 2014, **261**, 285–291.
11 J. Zhu and G. Chen, *J. Mater. Chem. A*, 2019, **7**, 5463–5474.
12 E. Cho, S.-W. Seo and K. Min, *ACS Appl. Mater. Interfaces*, 2017, **9**, 33257–33266.
13 C. Liang, R. C. Longo, F. Kong, C. Zhang, Y. Nie, Y. Zheng and K. Cho, *ACS Appl. Mater. Interfaces*, 2018, **10**, 6673–6680.
14 J. C. Garcia, J. Bareño, J. Yan, G. Chen, A. Hauser, J. R. Croy and H. Iddir, *J. Phys. Chem. C*, 2017, **121**, 8290–8299.
15 L. Hong, L. Hu, J. W. Freeland, J. Cabana, S. Öğüt and R. F. Klie, *J. Phys. Chem. C*, 2019, **123**, 8851–8858.
16 V. Galakhov, M. Neumann and D. Kellerman, *Appl. Phys. A: Mater. Sci. Process.*, 2009, **94**, 497–500.
17 D. Ensling, A. Thissen, S. Laubach, P. C. Schmidt and W. Jaegermann, *Phys. Rev. B: Condens. Matter Mater. Phys.*, 2010, **82**, 195431.
18 D. Ensling, G. Cherkashinin, S. Schmid, S. Bhuvaneswari, A. Thissen and W. Jaegermann, *Chem. Mater.*, 2014, **26**, 3948–3956.
19 S. Laubach, S. Laubach, P. C. Schmidt, D. Ensling, S. Schmid, W. Jaegermann, A. Thißen, K. Nikolowski and H. Ehrenberg, *Phys. Chem. Chem. Phys.*, 2009, **11**, 3278–3289.

20 K. Akada, T. Sudayama, D. Asakura, H. Kitaura, N. Nagamura, K. Horiba, M. Oshima, E. Hosono and Y. Harada, *Sci. Rep.*, 2019, **9**, 1–7.
21 H. Kiuchi, K. Hikima, K. Shimizu, R. Kanno, F. Toshiharu and E. Matsubara, *Electrochem. Commun.*, 2020, **118**, 106790.
22 S. Kurosumi, N. Nagamura, S. Toyoda, K. Horiba, H. Kumigashira, M. Oshima, S. Furutsuki, S.-I. Nishimura, A. Yamada and N. Mizuno, *J. Phys. Chem. C*, 2011, **115**, 25519–25522.
23 S. Kurosumi, K. Horiba, N. Nagamura, S. Toyoda, H. Kumigashira, M. Oshima, S. Furutsuki, S.-I. Nishimura, A. Yamada and N. Mizuno, *J. Power Sources*, 2013, **226**, 42–46.
24 K. Akada, T. Sudayama, D. Asakura, H. Kitaura, N. Nagamura, K. Horiba, M. Oshima, E. Hosono and Y. Harada, *J. Electron Spectrosc. Relat. Phenom.*, 2019, **233**, 64–68.
25 *SHAPE, V7.4*, 1987, **https://www.shapesoftware.com**.
26 E. Stavitski and F. M. De Groot, *Micron*, 2010, **41**, 687–694.
27 K. Horiba, Y. Nakamura, N. Nagamura, S. Toyoda, H. Kumigashira, M. Oshima, K. Amemiya, Y. Senba and H. Ohashi, *Rev. Sci. Instrum.*, 2011, **82**, 113701.
28 J. Akimoto, Y. Gotoh and Y. Oosawa, *J. Solid State Chem.*, 1998, **141**, 298–302.
29 M. Abbate, J. Fuggle, A. Fujimori, L. Tjeng, C. Chen, R. Potze, G. Sawatzky, H. Eisaki and S. Uchida, *Phys. Rev. B: Condens. Matter Mater. Phys.*, 1993, **47**, 16124.
30 L. Montoro, M. Abbate and J. Rosolen, *Electrochem. Solid-State Lett.*, 2000, **3**, 410.
31 D. Schmeißer, S. Schmidt, G. Seibold, G. Cherkashinin and W. Jaegermann, *ECS Trans.*, 2010, **25**, 37.
32 M. Gauthier, T. J. Carney, A. Grimaud, L. Giordano, N. Pour, H.-H. Chang, D. P. Fenning, S. F. Lux, O. Paschos and C. Bauer, *J. Phys. Chem. Lett.*, 2015, **6**, 4653–4672.

